Tech Science Press

Influence of the Axial Position of the Guide Vane on the Fluctuations of Pressure in a Nuclear Pump

Xiaorui Cheng[1,2,*], Yimeng Jiang[1], Min Li[1] and Shuyan Zhang[1]

[1]College of Energy and Power Engineering, Lanzhou University of Technology, Lanzhou, 730050, China
[2]Key Laboratory of Fluid Machinery and Systems of Gansu Province, Lanzhou, 730050, China
*Corresponding Author: Xiaorui Cheng. Email: cxr168861@sina.com
Received: 21 March 2020; Accepted: 24 August 2020

Abstract: The influence of the axial mount position of the guide vane on the pressure fluctuation in a nuclear pump (AP1000) is investigated. The characteristics of the three-dimensional flow inside the nuclear pump are analyzed by means of numerical simulation. Results indicate that when the axial relative distance between the guide vane and the pumping chamber is reduced, in conditions of "small flow," the efficiency of the pump increases, the pressure inside the pumping chamber decreases, while the losses related to the guide vane grow. Under large flow conditions, as the efficiency of the pump decreases, the losses for the guide vane and the pumping chamber increase. The pressure fluctuation in the annular pumping chamber is basically determined by the rotation frequency and the blade passing frequency. The magnitude of these fluctuations is affected by the guide vane axial position. In particular, the smallest possible amplitude is obtained when the outlet central plane of the guide vane coincides with the outlet axis of the pumping chamber.

Keywords: Nuclear main pump; guide vane; axial position; pressure fluctuation

1 Introduction

As the nuclear reactor coolant main circulation pump in the nuclear power plant, nuclear main pump is the first-class equipment on nuclear safety. Its stable operation is of great significance to the safety production of nuclear power plant. The working performance and safety of the nuclear main pump have received widespread attention. At present, vibration and noise caused by pressure fluctuation are common problems in the operation process of the nuclear main pump [1–3]. Many factors can induce the pressure fluctuation, and the interaction between the rotor-stator components is an important cause of the pressure fluctuation. Many scholars at home and abroad have studied this. Zhang et al. [4,5] examined the vibration frequency caused by rotor-stator interaction between the impeller and the volute of the pump, and obtained that the blade passing frequency and its multiple play a leading role in the vibration induced by pressure fluctuation. Cheng et al. [6] studied the effect of different rotor cantilever ratios on the hydraulic vibration of the nuclear main pump through the one-way fluid-solid coupling method. They found that the natural frequency of the rotor system can be effectively reduced by fluid-solid coupling. Zhu et al. [7] pointed out that blade passing frequency is the main factor causing the rotor-stator

interaction between the guide vane and the impeller in the nuclear main pump, serious pressure fluctuation generally occurred at the inlet and outlet of the guide vane. Li et al. [8] studied the interference of the impeller and guide vane on the flow field, the results show that the number of impeller blades affects the pressure fluctuation period and the interference of the impeller trailing edge on the flow field inside the guide vane is the main factor causing the pressure fluctuation in the guide vane. Wang et al. [9] also confirmed that the number of blade and guide vane affects the fluctuation cycle. Su et al. [10] analyzed the variation of the pressure fluctuation and radial force of the nuclear main pump during startup, and found that the pump which deviates from the design condition will cause the pressure fluctuation of the guide vane channel to increase and produce stronger radial vibration. Cheng et al. [11,12] found that the circumferential position of the guide vane has a significant influence on the pressure fluctuation in the pump through the full three-dimensional numerical calculation. They also analyzed the influence of the matching position between annular shell and guide vane on the distribution of pressure in the nuclear main pump and found that altering the guide vane position advisably can decrease the peak pressure fluctuation in the outlet of impeller. As a key part connecting the impeller and the pumping chamber, guide vane directly impacts internal flow of the flow passage component, which in turn affects the performance of the pump [13–15]. Cheng et al. [16] found that the wrap angle of the space guide vane has a significant effect on the flow field of the submersible well pump. Properly increasing the wrap angle can improve the characteristics of the airflow, reduce the turbulence loss and increase the energy conversion rate inside the guide vane.

In addition, the relative position between the flow passage components will also affect the flow characteristics of the fluid which is passing through it, causing pressure fluctuation. Dai et al. [17] conducted research and found that under different tip clearances, the pressure fluctuations in the flow field showed significant periodic changes. The pressure gradient of the engine pump will also change periodically as the impeller rotates. But there is currently little research in the influence of the relative position of the million-kilowatt-class nuclear main pump flow passage components on its hydraulic performance. In this paper, three different guide vane axial mount position are designed for this point. Adopting the RNG k–ε turbulence model to perform numeral calculation of unsteady flow and analyzing the influence of the axial relative position of the guide vane and the pumping chamber on the pressure fluctuation of the nuclear main pump pumping chamber. A reference scheme for optimization design of the nuclear main pump guide vane is provided.

2 Geometric Model and Scheme Design

2.1 Geometric Model and Grid Arrangement

In the present study, an AP1000 nuclear main pump was selected as the research object, the structure diagram is shown in Fig. 1. According to the similarity theory, the geometric parameters of the prototype pump are reduced to the parameters of the model pump for numerical calculation, proportional coefficient λ was defined as 0.4 by geometric similarity. The main designing parameters of model pump are: head H = 17.8 m, flow Q = 1145 m^3 / h, speed n = 1750 rpm. Working media is water temperature. Fig. 2a is a structure diagram of model pump flow passage components. Fig. 2b is a scaled model of pump fluid calculation domain profile. The entire water includes suction chamber, impeller, guide vane, pump shell, and inlet and outlet extension section.

Due to the complex structure of nuclear main pump, unstructured tetrahedral grid with strong inclusiveness to complicated boundaries will be used to divide the entire fluid region. And locally encrypt the impeller and guide vane to adjust the quality of the grid unit. The average expected y+ value of the impeller and guide vane blades is 31, which meets the requirements for solving the wall functions. Through the check of grid independence as shown in Tab. 1, the total number of grid points is 6.25×10^6, the number of passage parts as shown in Tab. 2. The calculation domain and the local grid is shown in Fig. 3.
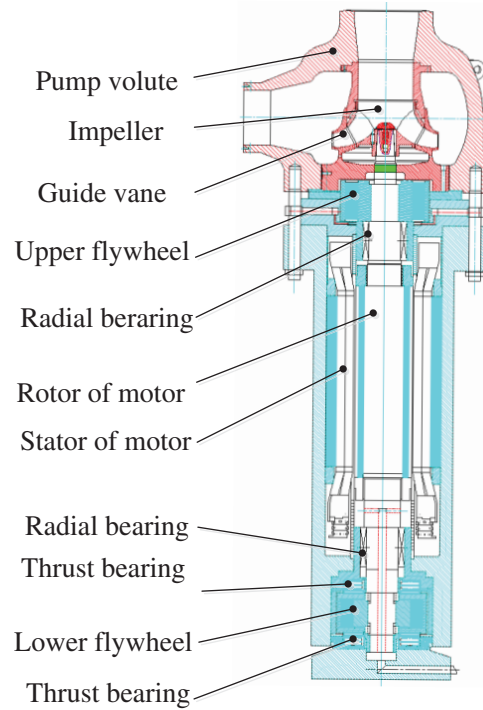
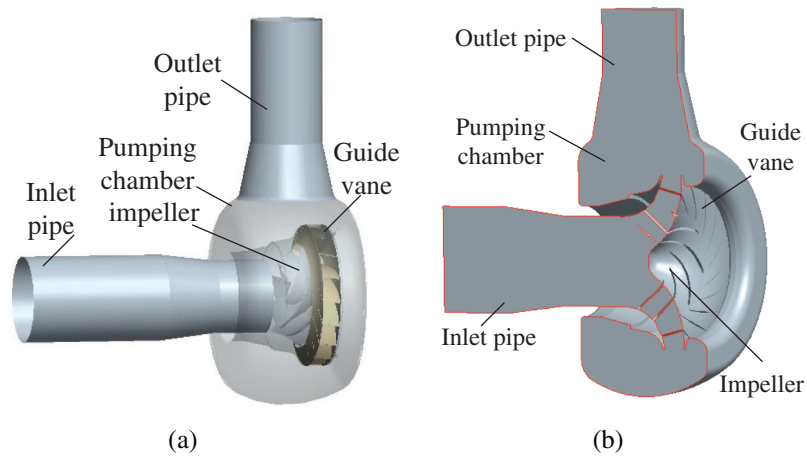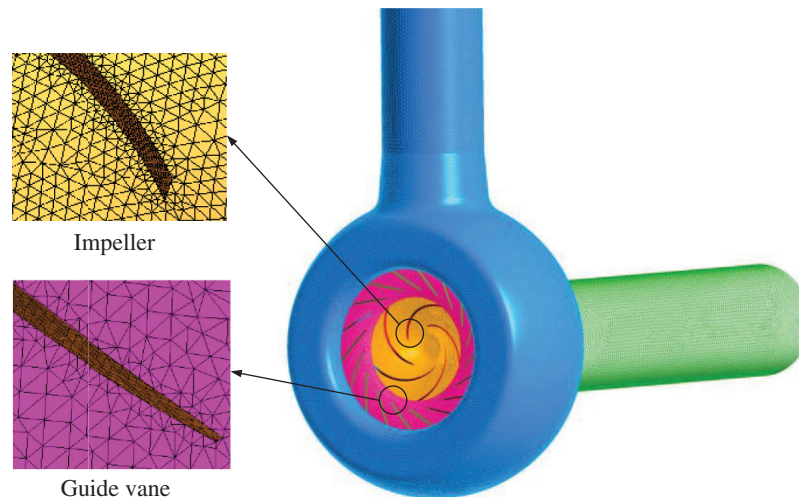**Figure 1:** Structure diagram of nuclear main pump

Figure 2: Three-dimensional structure and fluid domain schematic diagram of nuclear main pump. a. Nuclear main pump structure, b. Fluid calculation domain

Table 1: Grid-independent verification

Total number of grid points ($\times 10^4$)	255	399	537	625	721	864
Total head H (m)	22.7	22.5	22.3	22.0	22.0	22.0
Efficiency (%)	85.7	85.6	85.3	85.1	85.1	85.1

Table 2: Grid points number of hydraulic components

Hydraulic components	Inlet section	Impeller	Guide vane	Annular casing	Outlet section	Total
Grid points number ($\times 10^3$)	810	1900	1510	1600	430	6250

Figure 3: Grid generation schematic diagram of nuclear main pump model

2.2 Scheme Design

In this paper, based on the comprehensive consideration of the safety and structural permission of the pump, three axial mount positions of the guide vane are set, as shown in Fig. 4. For convenience of description, the distance between the guide vane and the pump outlet pipe axis in the direction of the impeller rotation axis which is simply referred to as the axial relative distance of the guide vane and the pumping chamber Δx. Different schemes correspond to different axial relative distance between guide vane and pumping chamber, as shown in Tab. 3.
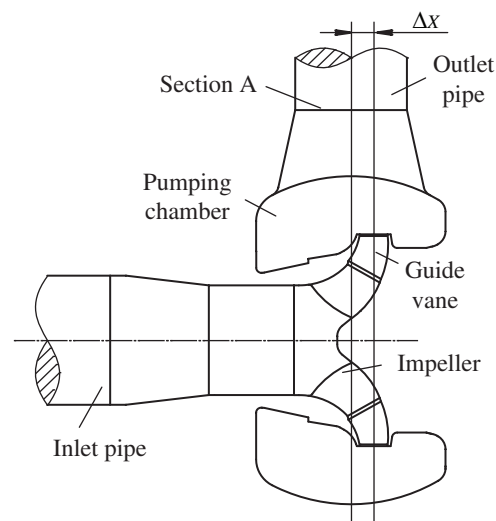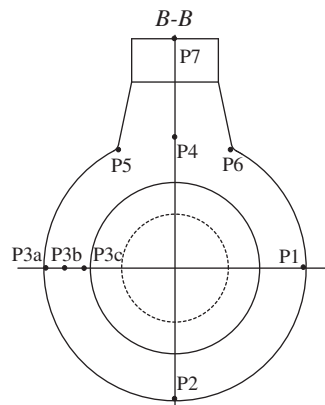
Figure 4: Schematic diagram of guide vane in different mount positions

Table 3: Design scheme information

Scheme	Scheme A	Scheme B	Scheme C
Δx/mm	89	44.5	0

To study the effect of the axial mount position of the guide vane on the pressure fluctuation in the pumping chamber, nine monitoring points were set on the mid-hight plane B-B of the outlet pipe of the pumping chamber. In the direction of fluid flow, four monitoring points P1, P2, P3a and P4 are set in the circumferential direction of the pumping chamber. Three monitoring points P3a, P3b and P3c are set radially. Three monitoring points, P5, P6 and P7 are set up at the tongue and outlet. The concrete position is shown in Fig. 5. The speed of the nuclear main pump impeller for this study is n = 1485 r/min, the number of blades is 5, so the rotation frequency is f_n = $n/60$ = 24.75 Hz, the blade passing frequency is f_r = $5f_n$ = 123.75 Hz.

Figure 5: Pumping chamber monitoring point distribution map

3 Numerical Method and Setting

3.1 Numerical Method and Boundary Conditions

Inside the nuclear main pump is a complex three-dimensional incompressible viscous turbulent flow. When performing numerical calculations on the nuclear main pump, ignoring the effect of medium temperature changes, the control equation of its three-dimensional flow field are:

(1) Continuity equation:

$$\frac{\partial u}{\partial x} + \frac{\partial v}{\partial y} + \frac{\partial w}{\partial z} = 0 \tag{1}$$

where, u, v, w are the components of the velocity vector in the three-dimensional coordinates x, y, z respectively.

(2) N-S equation of incompressible viscous fluid:

$$\frac{\partial}{\partial x_i}(u_i u_j) = f_i - \frac{1}{\rho}\frac{\partial p}{\partial x_i} + \mu \frac{\partial^2 u_i}{\partial x_i x_j} \tag{2}$$

where, P is the pressure on the fluid micro-body, f_i is the component of the mass force in the i direction.

The RNG k–ε turbulence model has been adopted as the computational procedure, which considers the flow separation inside the pump and has high accuracy in handling high strain rates and streamline flow. The pressure and momentum equations were coupled using the SIMPLEC algorithm with a high-resolution scheme. The finite volume method was used to discretize the governing equations, using a second-order scheme used for the advection term. In the RNG k–ε model, the transport equations for turbulent kinetic energy and dissipation rate are as follows [18]:

$$\frac{\partial(\rho k)}{\partial t} + \frac{\partial(\rho k u_i)}{\partial x_i} = \frac{\partial}{\partial x_i}\left[\alpha_k \mu_{\text{eff}} \frac{\partial k}{\partial x_j}\right] + G_k + \rho\epsilon \tag{3}$$

$$\frac{\partial(\rho \epsilon)}{\partial t} + \frac{\partial(\rho \epsilon u_i)}{\partial x_i} = \frac{\partial}{\partial x_i}\left[\alpha_\epsilon \mu_{\text{eff}} \frac{\partial \epsilon}{\partial x_j}\right] + \frac{C_{1\epsilon}}{k} G_k - C_{2\epsilon}\rho\frac{\epsilon^2}{k} \tag{4}$$

$$\mu_{\text{eff}} = \mu + \mu_t \tag{5}$$

$$\mu_t = \rho C_\mu \frac{k^2}{\epsilon} \tag{6}$$

where, C_μ, α_k and α_ε are empirical coefficients, ε is turbulent dissipation rate, $C_{1\varepsilon}$ and $C_{2\varepsilon}$ are empirical constants, taking 1.42, 1.68 respectively.

The inlet boundary condition is set to the velocity inlet, and the velocity was determined through the uniform normal flow running into the pump at suction section. The outlet was set to outflow and the stationary walls were set as no slip walls. The multi-reference coordinate system is used to calculate the steady uncompressible flow field. The impeller was set to a rotation domain with a rotation speed of $n = 1750$ r/min, the rest of the components are set to the static domain. Regarding the treatment of near wall problems, choose the standard wall functions unique to the RNG k-ε turbulence model. By observing that the outlet pressure tends to be stable or the convergence residual value is less than 10^{-5}, it is determined that the solution has converged [19]. Taking the steady calculation results as the initial conditions, and using unsteady calculations to analyse the pressure fluctuation, setting the time step to 2.857×10^{-4} s and calculating a total of 6 cycles. Taking the data of the last cycle for processing and analysis.

The pressure change law of the nuclear main pump can be directly reflected by the pressure fluctuation coefficient C_P, and C_P is defined as:

$$C_P = \frac{P - \overline{P}}{\frac{1}{2}\rho u_2^2} \tag{7}$$

$$u_2 = \frac{\pi D n}{60} \tag{8}$$

For which P represent the instantaneous pressure of the monitoring points, $\overline{P}$ represent the time-average pressure at one rotating revolution of the impeller, ρ represent the working media density, and u_2 is the circular velocity of the middle flow line at the impeller outlet.

The pressure fluctuation amplitude is defined as:

$$C_A = Cp_{max} - Cp_{min} \tag{9}$$

In order to comprehensively, accurately and quantitatively analyse the characteristics of pressure fluctuation, based on the pressure fluctuation coefficient C_P, the pressure fluctuation intensity I_{Cp} is defined for analysis. The expression is as follows:

$$I_{C_P} = \sqrt{\frac{1}{N}\sum_{n=0}^{N} C_P{}^2}, N = 120 \tag{10}$$

3.2 Numerical Accuracy Validation

Fig. 6 is experimental setup sketch of nuclear main pump model. The experimental setup is a closed class B precision test bench, and equipped with electromagnetic flowmeter with an accuracy of ±1.0%, inlet and outlet pressure sensor with an accuracy of ±0.1%. It also equipped with torque-speed transducer and instrument between pump and motor (the measurement accuracy is ±0.3%), pump flow, inlet and outlet pressure, speed and power can be read directly. The pump head and efficiency are calculated by measuring the inlet and outlet pressures, flow rates and torque of the pump. The head formula of the pump is:

$$H = \left(\frac{p_2}{\rho g} - \frac{p_1}{\rho g}\right) + \left(\frac{v_2^2}{2g} - \frac{v_1^2}{2g}\right) + (Z_2 - Z_1) \tag{11}$$

where H is head, m; Z is position head, m; P is pressure, Pa; v is velocity, m/s; ρ is fluid density, kg/m^3, subscript 1 indicates pump inlet, subscript 2 indicates pump outlet (the reference plane is selected on the horizontal plane where the centerline of the pump shaft is located).

Figure 6: Sketch of experimental setup

The pump efficiency calculation formula is:

$$\eta = \frac{\rho g Q H}{1000P} \times 100\% \tag{12}$$

where Q is flow rate, m^3/s; H is head, m; P is input power, kW; ρ is fluid density, kg/m^3.

The numerical simulation results of the model pump are compared with the experimental results and the comparison results are shown in Fig. 7. As can be seen in Fig. 6, the numerical calculation results of the head and efficiency are higher than the experimental results under different working conditions. The numerical results are in good agreement with the experimental results under design condition, the error of head is not more than 2.95%, the error of efficiency is not more than 2.4%. The calculation error of head and efficiency increased under the condition of small flow and large flow, but the head and efficiency variation trend of experimental are consistent with the numerical results invariably. These show that the numerical calculation method adopted in this study has certain applicability and accuracy.
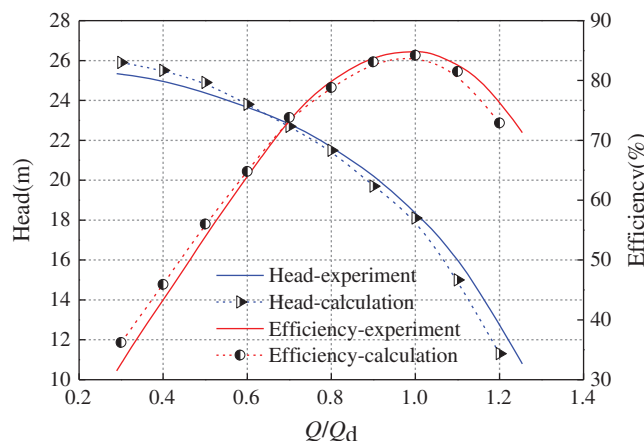
Figure 7: Characteristic curves of model pump

4 Results and Discussions

4.1 Effect of Guide Vane Axial Mount Position on the Flow inside the Pumping Chamber

The unstable flow in the pumping chamber is an important factor causing pressure fluctuation. In order to analyse the influence of the axial placement of the guide vane on the flow state inside the pumping chamber, an axial section A-A was established through the axis of the pump outlet pipe, as shown in Fig. 4. Fig. 8 is a streamline diagram of the A-A section when the nuclear main pump is placed at different axial positions of the guide vanes under the three operating conditions of 0.8 Q_d, 1.0 Q_d and 1.2 Q_d. It can be seen from the figure that the flow is complicated and the recirculation phenomenon is serious on A-A surface. This is mainly because the annular pumping chamber used in the nuclear main pump cannot ensure that the liquid flow in the pumping chamber conforms to the principle that the velocity moment is constant, which leads to the deterioration of the flow state in the pumping chamber. When the liquid flows from the guide vane outlet into the pumping chamber, a part of the fluid directly flows out from the pumping chamber outlet pipe in the upper area, and another part of the fluid flows from the upper side to the lower side in an annular flow around the pumping chamber channel, and finally flows out from outlet pipe of the pumping chamber. Therefore, the velocity in the upper area of the pumping chamber is significantly higher than the velocity in the lower side, and an obvious low-speed recirculation zone is formed in the lower area to increase the degree of recirculation.

Comparing the streamline diagrams under the three schemes under different working conditions, it can be found that as the axial distance between the guide vane and the pumping chamber decreases, the flow patterns on both sides of the guide vane gradually become uniform. At 0.8 Q_d, the flow in the pumping chamber is turbulent, the small vortex on the lower left side of the guide vane of Scheme A develops around, and the flow state at the upper left side of the guide vane near the outlet pipe of the pumping chamber is unstable, the magnitude and direction of the speed change obviously, forming a low-speed zone. Scheme B also has a low velocity zone near the outlet pipe of the pumping chamber. Unlike the first two schemes, the flow state of Scheme C is relatively stable, the velocity distribution near the outlet pipe of the pumping chamber is uniform, and the velocity gradient is relatively small. No obvious low-velocity regions similar to those described in Scheme A and Scheme B appear. In the 1.2 Q_d working condition, the low velocity zone is initially formed near the outlet pipe of the pumping chamber in Scheme A, and the flow pattern in other areas is improved compared with the designed working condition. Scheme B and scheme C have better flow pattern. From this, the flow pattern near the outlet pipe of the pumping chamber is relatively poor, prone to stronger pressure fluctuation.Reducing the axial relative distance between the guide vane and the pumping chamber can improve the flow state in the pumping chamber, and plays a good role in suppressing the recirculation in the pumping chamber, especially in the case of small flow conditions, the suppression effect on the recirculation is most obvious.
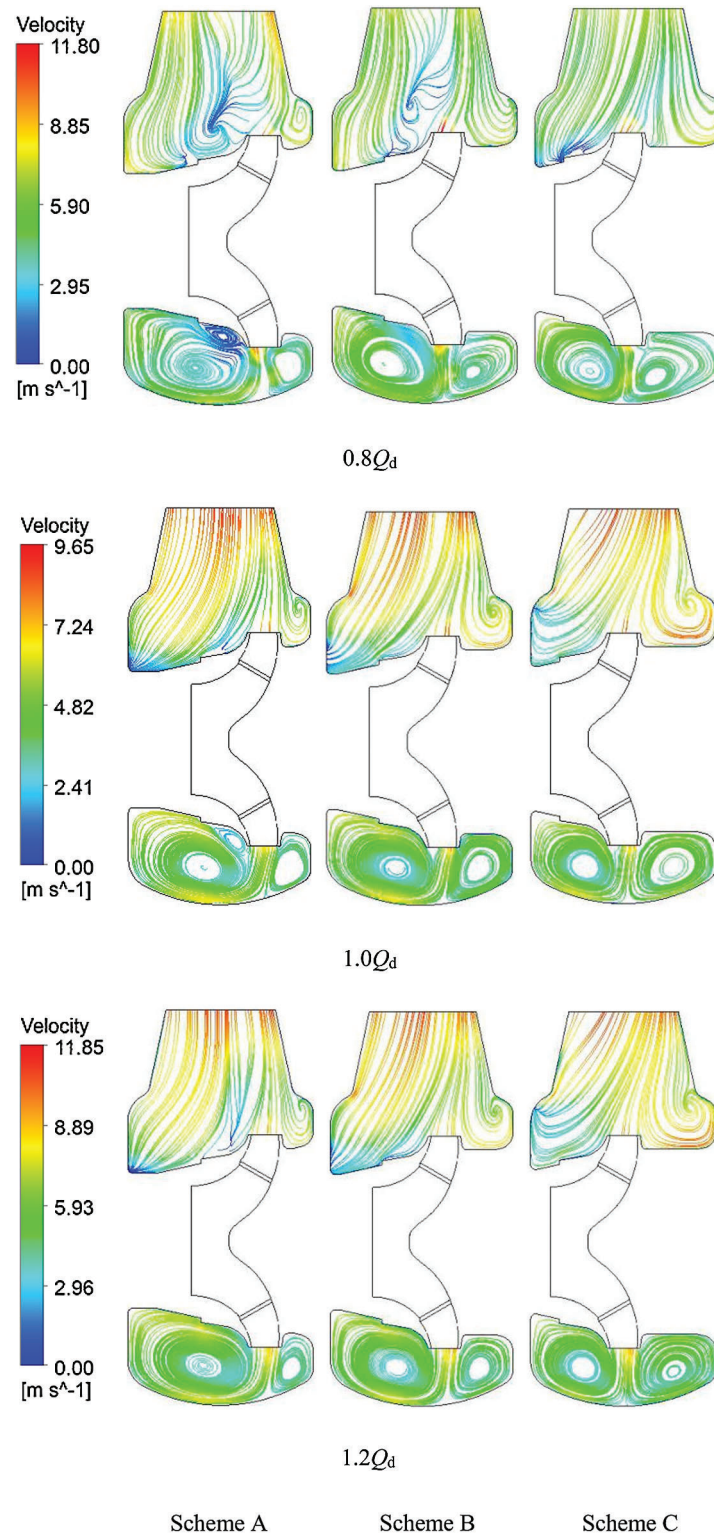
Figure 8: Streamline diagram of three schemes at *A-A* section a. Scheme A = 0.8 Q_d; b. Scheme B = 1.0 Q_d; c. Scheme C = 1.2 Q_d

4.2 Influence of Axial Mount Position of Guide Vane on Circumferential Pressure Fluctuation

Fig. 9 is a pressure fluctuation frequency domain diagram of the circumferential monitoring points in the annular pumping chamber at three different schemes. The figure reveals the dominant frequency of pressure fluctuation in three circumferential monitoring points appears at f_r or $14f_r$, at point P1, the dominant frequency of the three schemes are exactly twice the blade passing frequency. This demonstrates that the pressure fluctuation in the pumping chamber is mainly determined by the rotation frequency and the blade passing frequency. It can be seen from the amplitude analysis of the dominant frequency in three monitoring points P1, P2, P3a and P4, the pressure fluctuation of scheme A is the strongest and the amplitude of the dominant frequency is the largest in the four monitoring points at the circumferential direction. Except point P4, the dominant frequency amplitude of the scheme B is second, and the dominant frequency amplitude of the scheme C is the smallest. At point P4, the pressure fluctuation amplitude of the three schemes changes the most, while at other monitoring points, the amplitude fluctuation of the three schemes are relatively small. The main reason is that the axial relative distance between the guide vane and the pumping chamber directly determines the inflow position of the pumping chamber, and the inflow position of the pumping chamber directly affects the flow state at the junction of the pumping chamber and the outlet, the monitoring point P4 is located just at this junction, so it is greatly affected by the axial mount position of the guide vane. The other monitoring points which are located in the annular flow channel far from the junction of the pumping chamber and the outlet, the flow is relatively stable. Therefore, the pressure fluctuation is less affected by the axial mount position of the guide vane, and the amplitude of the dominant frequency changes little. From the above analysis, we can see that reducing axial relative distance Δx can reduce the pressure fluctuation amplitude of the circumferential monitoring point and effectively improve the flow state in the pumping chamber.
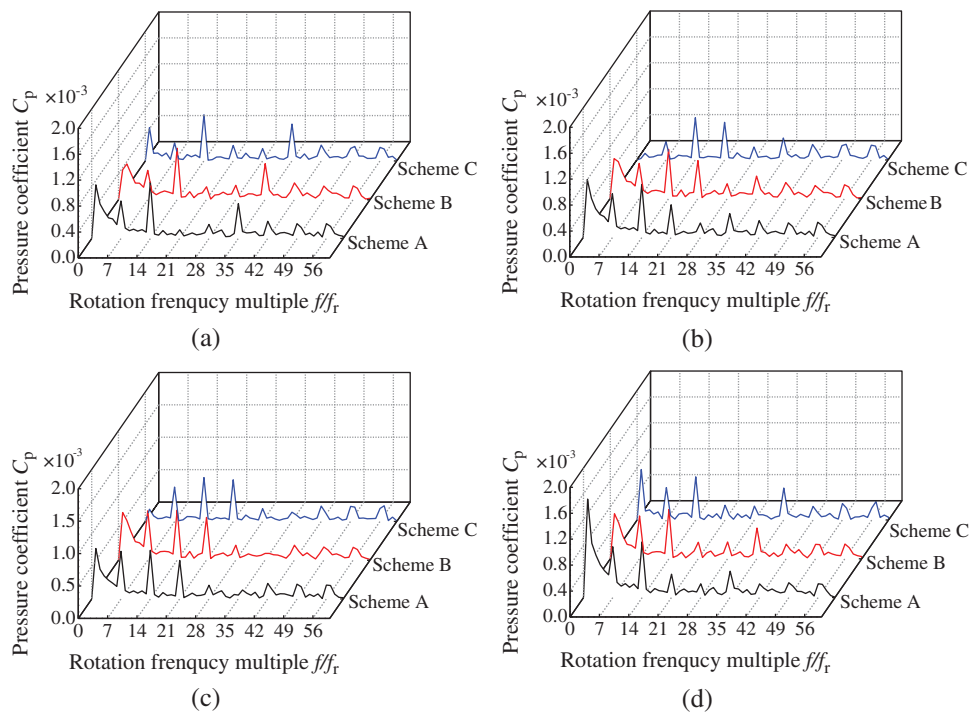

Figure 9: Circumferential pressure fluctuation frequency domain in the pumping chamber

In order to further analyse the pressure fluctuation characteristics, the pressure fluctuation amplitude and pressure fluctuation strength of the three schemes in the last rotation period are calculated, as shown in Fig. 10. It can be seen from the figure that the pressure fluctuation amplitude and the fluctuation intensity of the three schemes are consistent at the circumferential monitoring point, only the magnitude of the change is different. The variation of circumferential fluctuation amplitude and fluctuation strength of Scheme B and Scheme C is relatively flat, while the variation of Scheme A is relatively large, and the pulsation amplitude and pulsation intensity of Scheme A at point P4a are greatly increased. Except the point P3a, the pressure fluctuation amplitude and fluctuation intensity of the Scheme A are the largest, the Scheme B is the second, and the Scheme C is the smallest. Compared with the Scheme A, the pressure fluctuation amplitude at the four monitoring points of the Scheme C decreased respectively by 36.6%, 43.8%, 37.6% and 42.7%, and the pulsation intensity decreased by 29.1%, 39.1%, 27.4% and 42.2%, respectively. In summary, the pressure fluctuation at circumferential monitoring point of the Scheme A is the largest, and the pressure fluctuation is obviously weakened compared with the Scheme A, which indicates that the guide vane axial mount position affects the circumferential pressure fluctuation, particularly, the point P4 at the junction of the pumping chamber and the outlet has the greatest influence.
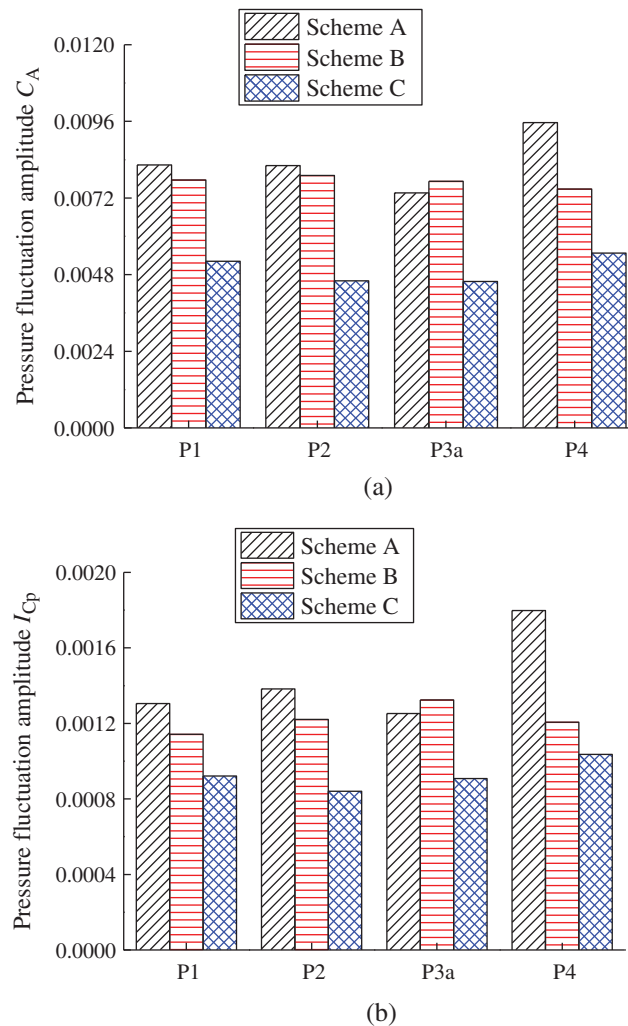

(a)

(b)

Figure 10: Circumferential pressure fluctuation amplitude and pressure fluctuation strength, (a) Pressure fluctuation amplitude, (b) Pressure pulsation intensity

4.3 Influence of Axial Mount Position of Guide Vane on Pressure Fluctuation at Tongue and Outlet

Fig. 11 displays the pressure fluctuation frequency domain at monitoring points P5, P6 and P7. It can be seen from the figure, similar to other monitoring points in the pumping chamber, the dominant frequency of pressure fluctuation in the three schemes P5, P6 and P7 are mainly determined by the rotation frequency and the blade passing frequency. Comparing and analysing amplitude of dominant frequency in the three schemes, we can see the axial mount position of guide vane affects the amplitude of the dominant frequency of points P5, P6 and P7, with the axial relative distance Δx decreases, the difference in the flow area on both sides of guide vane decreases, so that the flow patterns on both sides of guide vane gradually become uniform. Points P5 and P7 reveal that the amplitude in the dominant frequency of the pressure fluctuation also gradually decreases. The amplitude of the point P6 dominant frequency and the monitoring points P5 and P7 show the opposite law, that is, as the axial relative distance Δx decreases, the amplitude of dominant frequency of the pressure fluctuation gradually decreases. This is mainly because the point P6 is located near the splitting position of the annular pumping chamber, and the flow is extremely unstable and susceptible to other factors, which is due to the double action of the impact and reflux at the tongue. With the axial relative distance between the guide vane and the pumping chamber decreases, the distance between the point P6 and the guide vane outlet becomes smaller and smaller, and the corresponding impact of the point P6 is more obvious, and the pressure fluctuation amplitude increases. It can be seen from waveform of the frequency fluctuation that the pressure pulsation at the volute tongue and the outlet shows obvious dispersion, and the high frequency component of the blade passing double frequency increases, which is most obvious at the point P6. This is mainly due to the fact that the point P6 is relatively small from the guide vane outlet distance compared with the points P5 and P7, and accordingly the impeller double frequency effect is also increased.
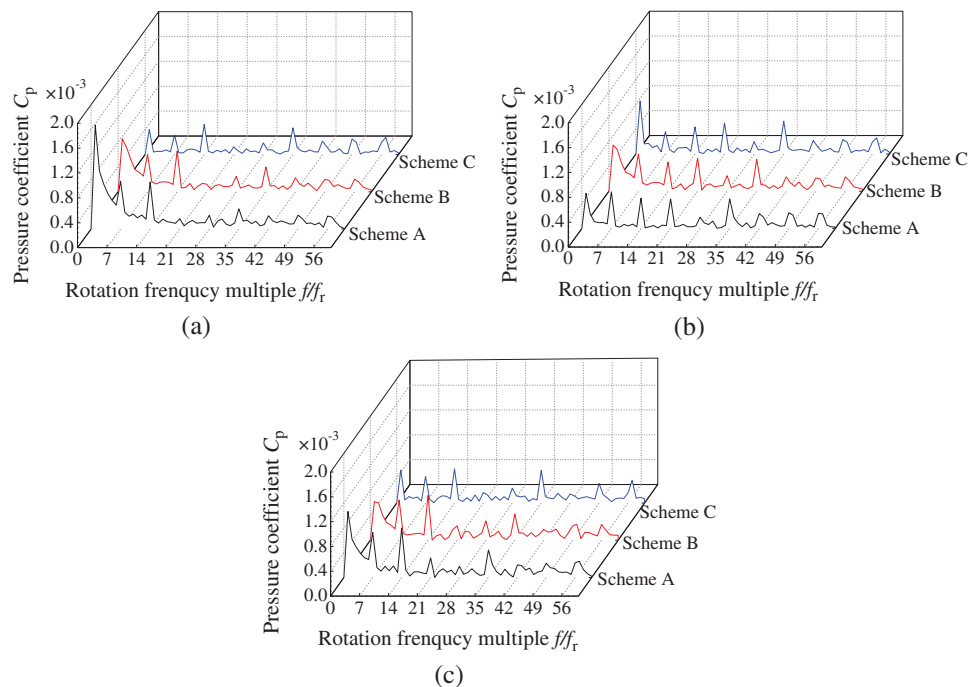

Figure 11: Pressure fluctuation frequency domain of points P5, P6 and P7

Fig. 12 shows the pressure fluctuation amplitude and pressure fluctuation strength at the tongue and outlet. As can be seen from the figure, at point P5, the pressure fluctuation amplitude and pressure

fluctuation strength of the three schemes are the largest, which is consistent with the change trend at point P7, the fluctuation amplitude and strength gradually decrease with the axial relative distance between the guide vane and the pumping chamber decreases. At point P6, the fluctuation amplitude and fluctuation strength of Scheme B are the largest, which in Scheme C is the smallest, and the fluctuation strengths of Scheme C and Scheme A are similar. It can be seen from the above analysis that the axial mount position of the guide vane affects the pressure fluctuation amplitude in the tongue and the outlet. Scheme C has the lowest pressure fluctuation amplitude and fluctuation strength, and the pressure fluctuation is the smallest, that is, when the outlet axis of the pumping chamber corresponds with the outlet central plane of the guide vane, the pressure fluctuation in the tongue and the outlet is minimal.
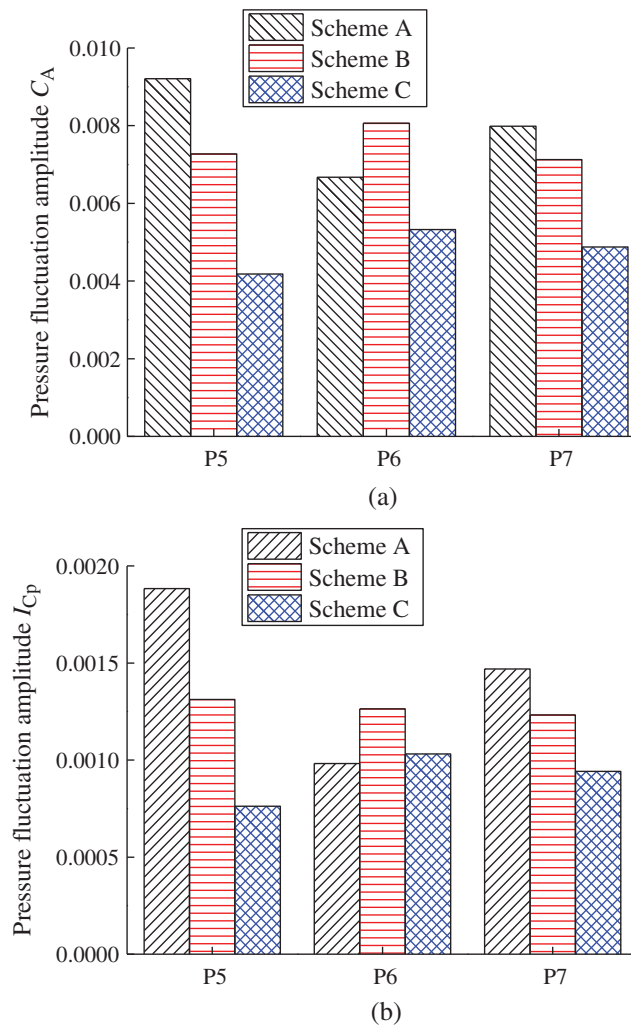

Figure 12: Pressure fluctuation amplitude and pressure fluctuation strength at points P5 ~ P7, (a) Pressure fluctuation amplitude, (b) Pressure fluctuation strength

5 Conclusion

(1) When the axial relative distance Δx is 89 mm, the model pump has the best hydraulic performance under design conditions and a shorter length of cantilever shaft. Reducing the axial relative distance between the guide vane and the pumping chamber, pump efficiency increases under low flow conditions, where

impeller efficiency increases, the flow state in the pumping chamber is improved, and the back-flow phenomenon is suppressed, thereby reducing the loss of the pumping chamber, but at the same time the guide vane loss is also increased; Under high flow conditions, the efficiency of the pump is reduced, in which the impeller efficiency is reduced, and the loss of the guide vane and the pumping chamber is correspondingly increased.

(2) The pressure fluctuation in the annular pumping chamber of the nuclear main pump is basically decided by the rotation frequency and the blade passing frequency, the variation of axial mount position of the guide vane mainly impacts the magnitude of pressure fluctuation amplitude. Reducing axial relative distance of the guide vane and the pumping chamber, the circumferential pressure fluctuation amplitude in the pumping chamber reduces correspondingly, in particular, the effect of pressure fluctuation at the junction between the pumping chamber and the outlet is most obvious.

(3) Pressure fluctuation at the tongue and outlet zone shows significant discreteness, the high frequency component of the frequency doubling of blade passing frequency increases. When the outlet central plane of guide vane corresponds with the outlet axis of the pumping chamber, the pressure fluctuation amplitude and the fluctuation strength at the tongue and the outlet are the smallest.

Conflicts of Interest: No potential conflict of interest was reported by the authors.

References

1. Lei, M. K., Chen, Y. X., Zhu, B., Hu, X. C. (2019). Pressure pulsation and its induced vibration of main coolant pumps in nuclear power plant. *Nuclear Power Technology, 12(3),* 0275–0205.

2. Rzentkowski, G., Zbroja, S. (2000). Acoustic characterization of a CANDU primary heat transport pump at the blade-passing frequency. *Nuclear Engineering and Design, 196(1),* 63–80. DOI 10.1016/S0029-5493(99)00235-6.

3. Cheng, X. R., Fu, L., Bao, W. R. (2018). Effect of cavitation flow on energy transfer in nuclear main pump. *Journal of Drainage and Irrigation Machinery Engineering, 36(5),* 369–376.

4. Zhang, D. S., Shi, W. D., Chen, B., Guan, X. F. (2010). Unsteady flow analysis and experimental investigation of axial-flow pump. *Journal of Hydrodynamics, 22(1),* 35–43. DOI 10.1016/S1001-6058(09)60025-1.

5. Si, Q. R., Yuan, J. P., Yuan, S. Q., Wang, W. J., Zhu, L. et al. (2014). Numerical investigation of pressure fluctuation in centrifugal pump volute based on SAS model and experimental validation. *Advances in Mechanical Engineering, 6,* 972081–972012. DOI 10.1155/2014/972081.

6. Cheng, X. R., Lv, B. R., Ji, C. Y., Wang, X. Q., Zhang, S. Y. (2019). Influence of cantilever ratio on hydraulic vibration of nuclear main pump. *Atomic Energy Science and Technology, 53(4),* 673–681.

7. Su, S. Z., Wang, P. F., Xu, Z. B., Ruan, X. D., Kong, W. J. (2017). Study on pressure fluctuation and radial force during startup of reactor coolant pump. *Nuclear Power Engineering, 38(03),* 110–114.

8. Zhu, R. S., Long, Y., Fu, Q., Yuan, S. Q., Wang, X. L. (2014). Pressure pulsation of a reactor coolant pump under low flow conditions. *Journal of Vibration and Shock, 33(17),* 143–149.

9. Wang, X. L., Yuan, S. Q., Zhu, R. S., Fu, Q., Wang, J. G. (2014). Effect of the number of blades to the reactor coolant pump radial forceunder variable flow transition conditions. *Journal of Vibration and Shock, 33(21),* 51–59.

10. Li, Y. B., Li, R. N., Wang, X. Y., Bi, Z., Hu, P. L. et al. (2015). Transient effects for flow interaction in the flow field of nuclear main pump. *Proceedings of the CSEE, 35(04),* 922–928.

11. Cheng, X. R., Jia, C. L., Yang, C. X., Lan, X. G. (2016). Influence of circumferential position of guide vane on unsteady flow characteristics in reactor coolant pump. *Journal of Mechanical Engineering, 52(15),* 197–204. DOI 10.3901/JME.2016.16.197.

12. Cheng, X. R., Wang, P., Zhang, S. Y. (2019). Investigation on matching characteristics of nuclear main pump guide vanes and annular casing. *Journal of the Brazilian Society of Mechanical Sciences and Engineering, 41(9),* 42. DOI 10.1007/s40430-019-1854-0.

13. Li, Z. L., Xu, S. L., Guan, Z. Q. (2018). Dynamic analysis of the axial vibration of the impeller in a reactor coolant pump induced by the radial leakage flow. *Chinese Journal of Computational Mechanics, 35(4),* 458–465.

14. Zhu, R. S., Cai, Z., Wang, X. L., Lu, Y. G., Chen, Z. L. et al. (2018). Cavitation characteristics and dynamic characteristics of a nuclear main pump based on the layer constraint of blades. *Journal of Vibration and Shock, 37(10),* 35–42.

15. Ni, D., Yang, M., Gao, B., Zhang, N., Li, Z. (2017). Numerical study on the effect of the diffuser blade trailing edge profile on flow instability in a nuclear reactor coolant pump. *Nuclear Engineering and Design, 322,* 92–103. DOI 10.1016/j.nucengdes.2017.06.042.

16. Cheng, X. R., Chen, H. X., Wang, X. Q. (2019). Analysis of the impact of the space guide vane wrap angle on the performance of a submersible well pump. *Fluid Dynamics & Materials Processing, 15(3),* 271–284. DOI 10.32604/fdmp.2019.07250.

17. Dai, J., Mou, J., Liu, T. (2020). Influence of tip clearance on unsteady flow in automobile engine pump. *Fluid Dynamics & Materials Processing, 16(2),* 161–179. DOI 10.32604/fdmp.2020.06613.

18. Gabbar, H. A., Mba, C. U., Marchesiello, S., Fasana, A., Garibaldi, L. (2017). Anomaly detection in a reactor coolant pump flywheel system via pulse shape analysis. *Journal of Failure Analysis and Prevention, 17(6),* 1174–1181. DOI 10.1007/s11668-017-0355-7.

19. Wang, X. Y., Wang, C. X., Li, Y. B. (2009). Numerical study of flow characteristics in the impeller side chamber of centrifugal pump. *Transactions of the Chinese Society for Agricultural Machinery, 40(4),* 86–90.